Atmos. Chem. Phys., 8, 3999–4017, 2008
www.atmos-chem-phys.net/8/3999/2008/

Atmospheric Chemistry and Physics

Error analysis for CO and CH_4 total column retrievals from SCIAMACHY 2.3 μm spectra

A. M. S. Gloudemans, H. Schrijver, O. P. Hasekamp, and I. Aben

SRON Netherlands Institute for Space Research, Utrecht, The Netherlands

Received: 3 January 2008 – Published in Atmos. Chem. Phys. Discuss.: 11 March 2008
Revised: 3 July 2008 – Accepted: 3 July 2008 – Published: 25 July 2008

Abstract. A detailed sensitivity analysis of the Iterative Maximum Likelihood Method (IMLM) algorithm and its application to the SCIAMACHY 2.3 μm spectra is presented. The sensitivity analysis includes a detailed assessment of the impact of aerosols in the 2.3 μm range. Results show that near strong aerosol sources mineral dust and biomass aerosols can have an effect of ∼7–10% on the CH_4 total columns retrieved from this wavelength range if aerosol scattering is neglected in the retrieval algorithm. Similar but somewhat larger effects are found for CO, but due to the larger variability of CO these errors are less important. Away from strong sources much smaller effects of a few percent are found. Using CH_4 as a proxy for CO and/or including aerosol information in the retrieval algorithm significantly reduces these errors for both CO and CH_4. Spectroscopic uncertainties are mostly negligible except for uncertainties in the CH_4 intrinsic line intensities, which can be important. Application of the IMLM algorithm to the SCIAMACHY 2.3 μm spectra shows that the quality of the retrieved CO and CH_4 total columns is good, except for a bias for large instrument-noise errors which is partly due to remaining calibration issues. Polarization sensitivity of the SCIAMACHY instrument has a negligible effect on the retrieved CO and CH_4 total columns. The H_2O total columns, which have to be retrieved simultaneously with CO and CH_4 due to overlapping absorption lines, agree well with H_2O total columns from ECMWF data. This ensures that the fit to the H_2O absorptions is of sufficient quality not to hamper the retrieved CO and CH_4 total columns from SCIAMACHY spectra.

Correspondence to:
A. M. S. Gloudemans
(a.gloudemans@sron.nl)

1 Introduction

With the launch of the SCanning Imaging Absorption spectroMeter for Atmospheric CHartographY (SCIAMACHY)[1] on board the ENVISAT satellite in 2002 (Bovensmann et al., 1999) a new class of retrieval algorithms have been developed. SCIAMACHY is the first and currently the only satellite instrument that measures near-infrared spectra in the 1–2.4 μm spectral range from space at high spectral resolution. These measurements are sensitive down to the Earth's surface, which is of particular interest for measuring tropospheric gases. The SCIAMACHY near-infrared spectra contain atmospherically interesting molecules such as CH_4, CO_2, CO, and H_2O, of which the bulk resides in the troposphere. Retrieval algorithms applied to this wavelength range include the Weighting Function Modified-DOAS (WFM-DOAS) algorithm (Buchwitz et al., 2000; Buchwitz and Burrows, 2004; Buchwitz et al., 2004), the Iterative Maximum A Posteriori-DOAS (IMAP-DOAS) algorithm (Frankenberg et al., 2005b), and the Iterative Maximum Likelihood Method (IMLM) algorithm (Schrijver, 1999; Gloudemans et al., 2005).

The IMLM algorithm has been applied successfully to near-infrared SCIAMACHY spectra between 1–2.4 μm (e.g. Houweling et al., 2005; Gloudemans et al., 2005; de Laat et al., 2006; Gloudemans et al., 2006; de Laat et al., 2007). It is also used in sensitivity studies for future near-infrared satellite instruments with spectral channels around 2.3 μm (Jongma et al., 2006). A sensitivity study of an early version of the algorithm has been published by Schrijver (1999) but application to the SCIAMACHY spectra required significant updates of the algorithm resulting in version 6.3 which is used in de Laat et al. (2006), Gloudemans et al. (2006), and de Laat et al. (2007). Although these papers mention some sensitivity results a systematic error analysis is still lacking.

[1] http://envisat.esa.int/instruments/sciamachy/

Published by Copernicus Publications on behalf of the European Geosciences Union.

Such an analysis is important since an accuracy of ∼2% for CH_4 and ∼10–20% for CO is required in order to determine e.g., CH_4 sources and sinks, and to estimate CO emissions (e.g. Kelder et al., 2005; Ehret and Kiemle, 2005). Here, a detailed error analysis is presented for the 2.3 μm wavelength range, including sensitivity calculations of the impact of aerosols and SCIAMACHY polarization. In addition, the quality of the SCIAMACHY CO and CH_4 total columns from the IMLM algorithm is further assessed as well as remaining SCIAMACHY calibration issues, which have not been reported in Gloudemans et al. (2005). Section 2 describes the IMLM algorithm. Section 3 explores the quality of the SCIAMACHY CO, CH_4, and H_2O total columns retrieved with the IMLM algorithm and provides explanations for biases found. Section 4 shows the total column averaging kernels and sensitivity results for various parameters, including a priori profiles, spectroscopic parameters, aerosols, and polarization. Section 5 summarizes the conclusions.

2 Algorithm description

The retrieval method described here is based on an Iterative Maximum Likelihood Method (IMLM) and has been developed at SRON. The forward model includes the atmospheric absorption and the instrument characteristics. The algorithm uses a slightly different approach than most other retrieval algorithms for near-infrared trace gases, such as WFM-DOAS and IMAP-DOAS (Buchwitz et al., 2000; Frankenberg et al., 2005b) which convert the observed detector signal to reflectivities: the IMLM algorithm fits a model of the expected detector signal to the measurements by varying the total amounts of the trace gases that play a role in the selected retrieval window.

2.1 Forward model

The forward model includes two main components. The first component describes the atmospheric reflectance spectrum computed from the solar spectrum and absorption by the Earth atmosphere. In the second component this atmospheric spectrum is fed into an instrument model based on characterisation and calibration of the instrument in order to compute the expected measured signal. The instrument model described in this paper focusses on the characteristics of the SCIAMACHY near-infrared grating spectrometers, but characteristics of other (near-)infrared instruments can also be easily included in the instrument model (e.g. Jongma et al., 2006).

2.1.1 Radiative transfer

The atmospheric reflectance spectrum can be computed using the equation:

$$I(\nu) = I_0(\nu)e^{-\tau(\nu)}\cos(\theta)a(\nu)\pi^{-1}R_{\odot}^{-2}, \quad (1)$$

where a fixed value of the surface albedo a is used, assuming Lambertian reflection. I_0 is a model solar irradiance, $R_{\odot}$ the distance from the Sun, and θ the solar zenith angle. The solar spectrum used in the IMLM algorithm is a high-resolution Spacelab 3 ATMOS spectrum (http://remus.jpl.nasa.gov/atmos/ftp.sl3.sun.html). $\tau(\nu)$ is the absorption optical depth. Scattering in the atmosphere is not taken into account in the radiative transfer. The effects of this simplification on the retrieved total columns are presented in Sect. 4.5.

The absorption optical depth $\tau(\nu)$ is computed using a priori trace gas profiles and a first guess of the total columns of all trace gases present in the selected retrieval window. This first guess is updated after each iteration (see Sect. 2.2). Temperature and water vapour profiles are taken from data from the European Centre for Medium-Range Weather Forecasts (ECMWF)[2]. Three-hourly forecast data on a 0.5° by 0.5° grid have been interpolated to the satellite overpass time and foot print (cf. http://www.knmi.nl/samenw/tosti/). The trace gas profiles are assumed having a fixed dependence on pressure – with the pressure distribution coming from the ECMWF data – and are taken from the US standard atmosphere (Anderson et al., 1986).

The atmosphere is vertically divided in a number of layers with a thickness of 1 km up to an altitude of 25 km, 2.5 km between 25 and 50 km, and 5 km above 50 km altitude. Spectroscopic data are taken from the HITRAN molecular database, version 2004 (Rothman et al., 2005). The cross-section $\sigma(\nu)$ of each transition is then calculated from its line intensity and the Voigt line shape corresponding to the temperature and pressure of each layer on a sufficiently fine wavenumber grid, i.e. with a much higher spectral resolution than that of the satellite measurements to which the retrievals will be applied. In the case of SCIAMACHY which has a spectral resolution of 0.26 nm around 2.3 μm a wave number grid of 0.05 cm^{-1} has been used. For the j-th layer the partial optical density can then be written:

$$\tau_j(\nu) = \sum_k C_{jk}\sigma_k(\nu), \quad (2)$$

where $\sigma_k(\nu)$ is the absorption cross-section of a species k at frequency ν and C_{jk} is its partial column in the j-th layer. The partial columns C_{jk} can be expressed as a fraction g_{jk} of the total (slant) column $C_k = \sum_j C_{jk}$:

$$\tau_j(\nu) = \sum_k C_k g_{jk}\sigma_k(\nu). \quad (3)$$

The total optical density of the atmosphere is the sum over the optical densities of the individual layers:

$$\tau(\nu) = \sum_k C_k \sum_j g_{jk}\sigma_k(\nu). \quad (4)$$

This formulation presents an important advantage in case the trace gas profiles are kept constant during the retrieval except

[2] http://www.ecmwf.int

for an overall scaling factor. Then the fractions g_{jk} are not changing and the sum over j needs only be computed once at the start of the retrieval.

2.1.2 Instrument model

The resulting high-resolution reflectance spectrum I is then fed into a model of the instrument yielding the modelled detector counts. This model accounts for the wavelength dependent transmission of the optics, the dispersion by the grating, the conversion of the wavelength grid to detector pixels, the detector quantum efficiency, the analogue-to-digital conversion, and the thermal background and dark current.

The contents of the l-th detector pixel become

$$N_l = B_l + f_l Q_l \int_{\lambda_{\text{low}}}^{\lambda_{\text{high}}} d\lambda \int_{-\infty}^{\infty} d\lambda' V(\lambda - \lambda') T(\lambda') I(\lambda') \quad (5)$$

where I is the incoming radiance spectrum, T the (optical) transmittance, V the slit dispersion function, λ_{low} and λ_{high} the limits of the wavelength coverage of the l-th detector bin, Q the quantum efficiency, f the analogue-to-digital factor, B the total dark signal, and N the measured signal in binary units. This formulation assumes that there is no non-linearity in the process. Non-linearity effects on N can be modelled by first computing N as above and then applying the calibrated non-linearity correction.

In a numerical algorithm, the above integrations are replaced by summations, and the above expression can be written in matrix form

$$N = B + \mathbf{A}I. \quad (6)$$

The input radiance spectrum $\boldsymbol{I}$ is a vector of N_{spec} elements. The detector spectrum $\boldsymbol{N}$ and the total dark signal $\boldsymbol{B}$ are both vectors of N_{det} elements. The matrix $\mathbf{A}$ describes the total instrument transformation of the input spectrum $\boldsymbol{I}$ into detector counts. It is a sparse matrix of $N_{\text{det}} \times N_{\text{spec}}$ elements with only a broad diagonal of non-zero elements, whose width is determined by the slit dispersion.

If matrices $\mathbf{A}$ are precomputed for a given constellation of instrumental parameters, the main function of the instrument module can be implemented by a matrix multiplication. This represents a big gain in computing time, especially because the matrix multiplication can be restricted to the small fraction of non-zero elements in $\mathbf{A}$.

The instrument model also computes the expected measurement noise by evaluating the various contributing noise sources: photo-electron shot noise – from the incoming atmospheric spectrum, the thermal background, and the dark current –, Johnson noise, and detector read-out noise. The resulting noise depends on the pixel exposure time t and the co-adding factor F, corresponding to a total integration time of Ft. If a detector pixel measures a signal of N binary units (BU), including the thermal background and dark current, this corresponds to N/f photo-electrons, if f is the analogue-to-digital conversion factor from photo-electrons to BUs. Then the total noise of that detector pixel is

$$e_l = \sqrt{F(\varepsilon_{\text{ro}}^2 + t\varepsilon_{\text{J}}^2) + Nf}. \quad (7)$$

where ε_{ro} and ε_{J} are the electronics read-out and Johnson noise, respectively, expressed in BU.

2.1.3 Closure term and derivatives

The forward model is completed by a closure factor, a multiplicative factor in the shape of a low-order polynomial. The coefficients of the terms of this polynomial are additional fit parameters. The closure factor can correct for any low-frequency imperfection of the model. In particular the zero-order term is used to fit the model to the mean signal level, depending mainly on the effective surface albedo. The higher-order terms correct several possible deviations, such as continuum effects, low-frequency calibration effects, and variations of surface albedo with wavelength. In the $2.3\,\mu$m wavelength range a first order polynomial closure term is sufficient. Equation (6) then becomes

$$N' = B + \mathbf{PA}I, \quad (8)$$

where $\mathbf{P}$ is a diagonal matrix with the values of the closure factor for the detector pixels.

In addition, the forward model computes the derivatives of the expected counts with respect to the fitting parameters, i.e. the total columns and the terms of the polynomial closure term. The derivatives of N_l' with respect to total columns follow from Eqs. (8), (1), and (4):

$$\partial N'/\partial C_k = \mathbf{PA}\partial I/\partial C_k, \quad (9)$$

$$\partial I(\nu)/\partial C_k = -I_0(\nu) e^{-\tau(\nu)} \cos\theta a(\nu) \pi^{-1} R_{\odot}^{-2} \partial\tau(\nu)/\partial C_k, \quad (10)$$

and

$$\partial\tau(\nu)/\partial C_k = \sum_j g_{jk} z_k(\nu). \quad (11)$$

The derivatives with respect to the coefficients of the closure factor are simply proportional to the polynomial terms.

2.2 Fitting procedure

The fitting process aims at finding those values for the fit parameters $x = x_1 \ldots x_M$, i.e. the total trace gas columns and the coefficients of the polynomial closure term, that correspond to the maximum statistical likelihood for the measured detector counts within the measurement error $\boldsymbol{e}$:

$$\boldsymbol{S} = \boldsymbol{N}'(x) + \boldsymbol{e} \quad (12)$$

where $\boldsymbol{S}$ is the measurement vector with N_{det} elements. The forward model $\boldsymbol{N}'(x)$ is denoted as the vector $\boldsymbol{N}'(x) = N_1'(x_1 \ldots x_M) \ldots N_{N_{\text{det}}}'(x_1 \ldots x_M)$, also consisting of N_{det} elements N_n' each depending on the fit parameters x_m.

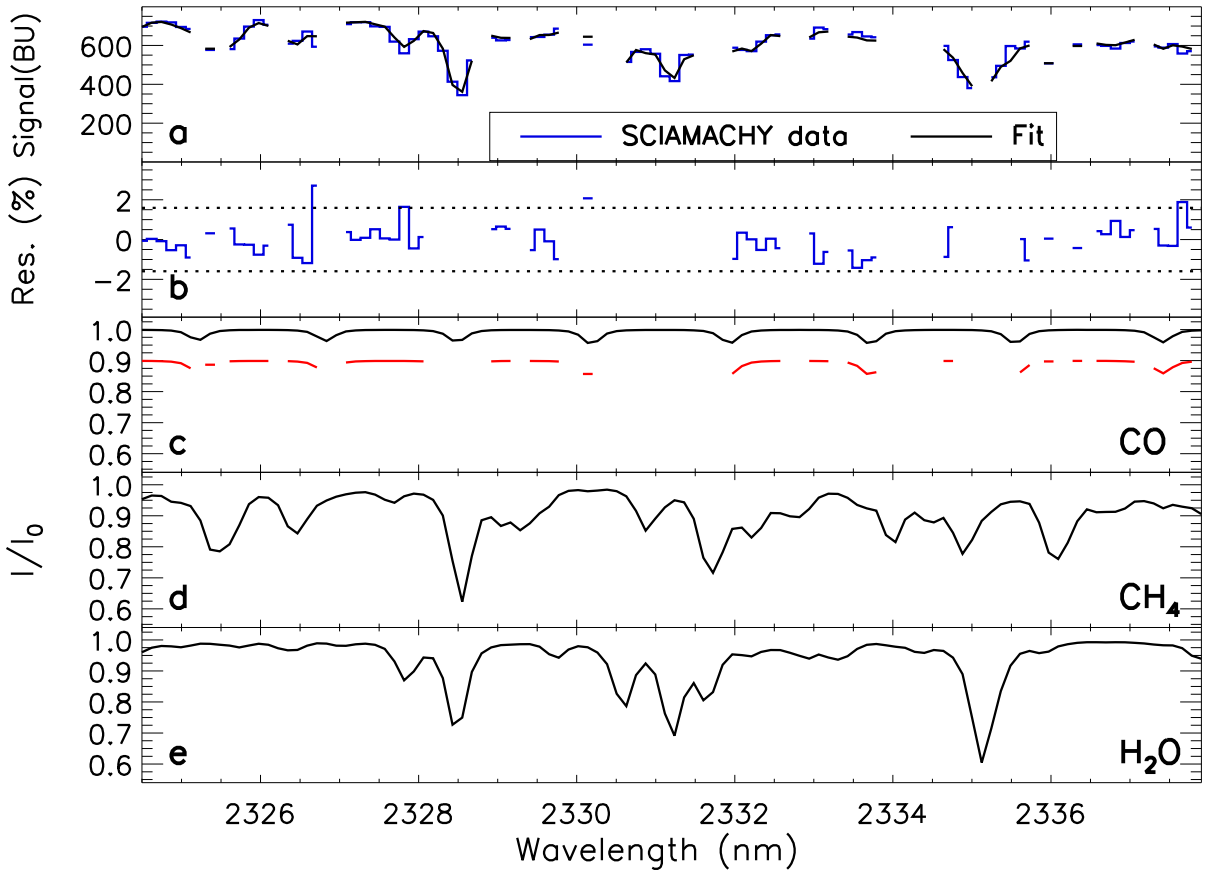

Fig. 1. SCIAMACHY 2.3 μm spectrum for 9 September 2003 over central Africa, illustrating the weak CO lines and the overlap with CH_4 and H_2O. **(a)** SCIAMACHY spectrum and fit, excluding damaged detector pixels. **(b)** Residuals, excluding detector pixels that are damaged or cover strong interfering H_2O lines. The dotted lines indicate +/− the mean noise level in this wavelength range. **(c)** CO fit for all detector pixels (black) and only for those used in the fit, as in (b) (red and offset by 0.1 for clarity). **(d)** CH_4 fit. **(e)** As (d), but for H_2O. The fit indicates a high CO total column of 4.1×10^{18} molec/cm^2, and CH_4 and H_2O columns of 3.5×10^{19} and 1.1×10^{23} molec/cm^2.

Because of the non-linear character of the model, Eq. (12) cannot be inverted directly, but the forward model can be linearized using a Taylor expansion. Neglecting the higher order terms this results in:

$$\boldsymbol{N'(x)} \approx \boldsymbol{N'(x_0)} + \mathbf{D}(\boldsymbol{x} - \boldsymbol{x_0}). \quad (13)$$

The vector x_0 contains the first guess values of the fit parameters and $\mathbf{D}=\partial \boldsymbol{N'(x)}/\partial \boldsymbol{x}|_{x_0}$ is the $N_{\mathrm{det}}\times M$ matrix with the derivatives.

Equation (13) can be solved with an iterative procedure where an updated value of the vector with the fit parameters is computed in the i-th iteration as

$$\boldsymbol{x}_{i+1} = \boldsymbol{x}_i + (\mathbf{D^T\Sigma^{-1}D})^{-1} \cdot \mathbf{D^T\Sigma^{-1}} \cdot (\boldsymbol{S} - \boldsymbol{N'(x}_i))^T \quad (14)$$

Here, $\mathbf{\Sigma}$ is the measurement covariance matrix, which is a diagonal matrix based on the noise of the individual detector pixels. Note that this is equivalent to a weighted least-squares fit. The covariance of the estimated parameters, i.e. $(\mathbf{D^T\Sigma^{-1}D})^{-1}$, gives the error due to the measurement noise $\boldsymbol{e}$.

The retrieval results are independent of the starting values for the total trace gas columns, which can thus be conveniently taken as zero. Convergence is always reached within 4 iteration steps.

3 SCIAMACHY retrievals

This section shows the application of the IMLM retrieval algorithm to the SCIAMACHY 2.3 μm spectra which contain absorption lines of the atmospheric trace gases water vapour (H_2O), carbon monoxide (CO), and methane (CH_4) (see Fig. 1). The most important issues complicating the retrieval of CO and other gases from these SCIAMACHY spectra are the ice layer growing onto the near-infrared detectors, the variation of the dark signal within an orbit, and the increasing number of damaged detector pixels as discussed in

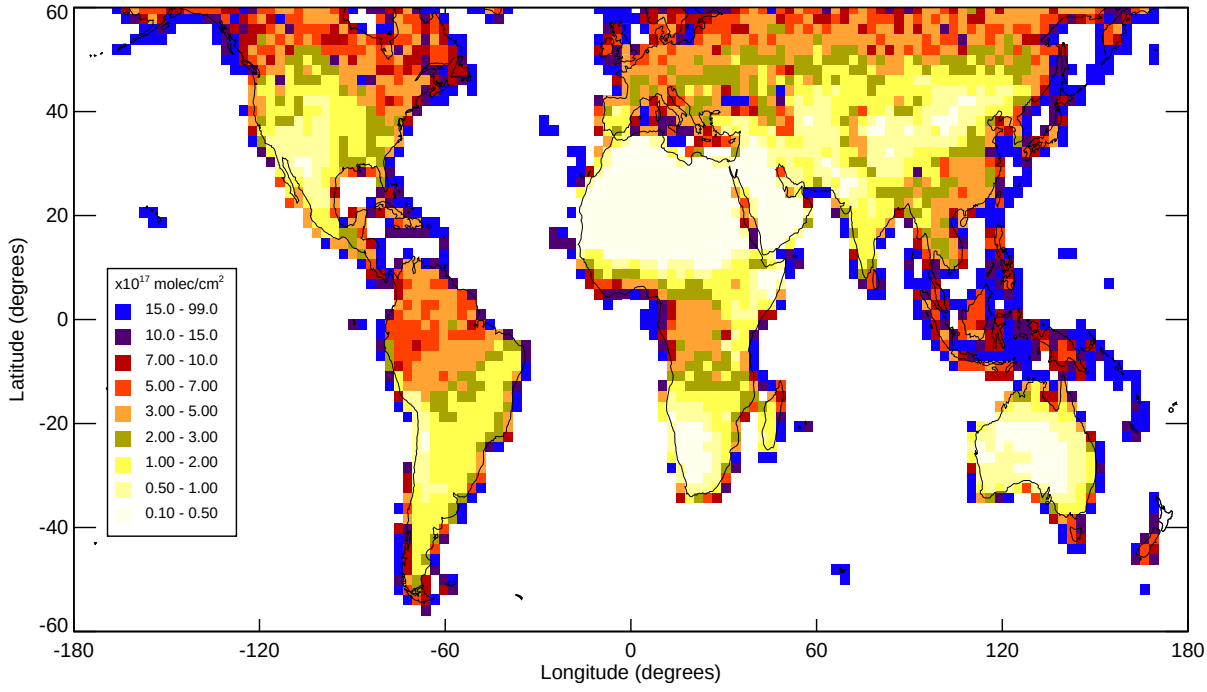

Fig. 2. Global distribution of the average SCIAMACHY CO monthly-mean instrument-noise error for the year 2004 using the same data set as in de Laat et al. (2006, 2007). Note that large instrument-noise errors are found in coastal regions. This is due to the fact that those SCIAMACHY measurements partially occur over sea and the surface albedo over sea is much lower than over land resulting in larger instrument-noise errors than land-only measurements.

detail by Gloudemans et al. (2005). They show that including a detailed correction for the ice layer and using an improved calibration significantly reduces the errors in the retrieved CO and CH_4 total columns. This improved calibration is taken from the SRON database set up by Kleipool (Kleipool, 2003a,b, 2004a,b) and is the same as those included in the SCIAMACHY level 1b products patched by SRON[3]. After correction for these major issues, de Laat et al. (2007) show that the instrument-noise error is the dominant error source of the retrieved CO total columns and that this noise error has a large spatial variation. Figure 2 shows the global distribution of the CO instrument-noise error for the year 2004 which is similar to that shown in (de Laat et al., 2006, 2007) for a somewhat different time period. The instrument-noise error and some remaining minor SCIAMACHY calibration issues are discussed below in more detail. The results are obtained from the same retrieval version 6.3 as used by de Laat et al. (2006), Gloudemans et al. (2006), and de Laat et al. (2007) and uses the same retrieval window which ranges from 2324.5 to 2337.9 nm, containing the strongest *R*-branch lines of the CO first overtone band.

[3]http://www.sron.nl/~richardh/SciaDC/scia_patch_1b/index.html

3.1 SCIAMACHY instrument-noise error

3.1.1 Instrument-noise error trends

The noise of the SCIAMACHY spectra is calculated with Eq. (7) using in-orbit and preflight measurements for the different noise terms. The co-adding factor F is always equal to 1 for SCIAMACHY 2.3 μm spectra. The instrument-noise error in the retrieved trace gas columns depends on the signal-to-noise ratio of the spectra, which strongly depends on surface albedo and solar zenith angle as has already been shown for CO by de Laat et al. (2006, 2007). Figure 3 shows the dependence of the instrument-noise error on the retrieved surface albedo for CO and CH_4 in SCIAMACHY's 2.3 μm spectra.

In the fitting procedure described in Sect. 2.2 noisy detector pixels contribute less to the best fit to the spectrum than less noisy pixels. In the case of SCIAMACHY this is an important issue, especially for weak absorbers such as CO, since degradation of detector pixels is a common phenomenon in the near-infrared channels of SCIAMACHY (Kleipool et al., 2007). de Laat et al. (2006, 2007) show that the precision of the SCIAMACHY CO total columns is determined by the instrument-noise error and thus is an important quantity for CO total column retrievals. One of their findings is an unrealistically large positive bias for instrument-noise

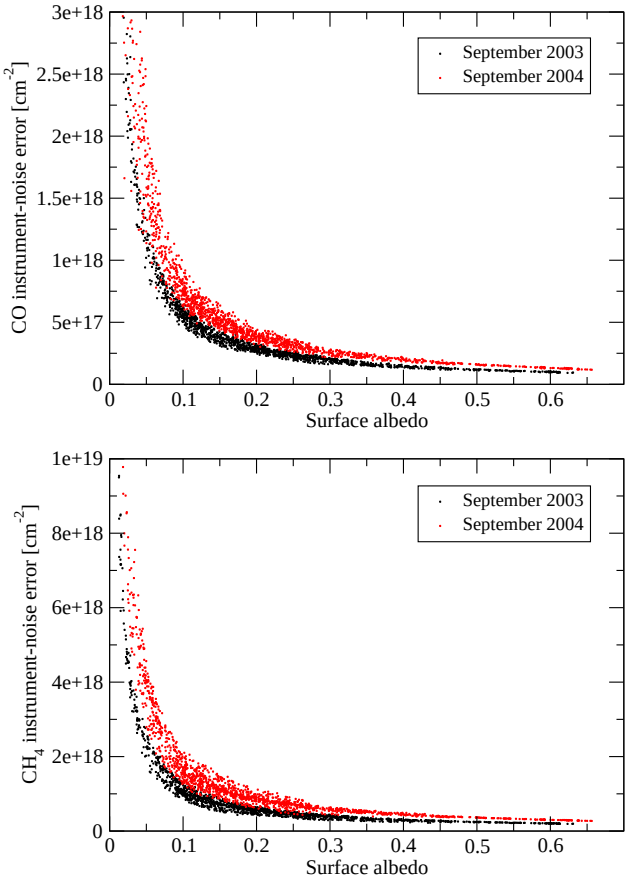

Fig. 3. Random instrument-noise errors in the CO (upper panel) and CH_4 (lower panel) total columns retrieved from SCIAMACHY's 2.3 μm spectra as function of retrieved surface albedo for two dates: September 2003 (shortly after decontamination) and September 2004 (two months after decontamination). The ice layer grows over time and reduces the transmission and thus the signal-to-noise ratio.

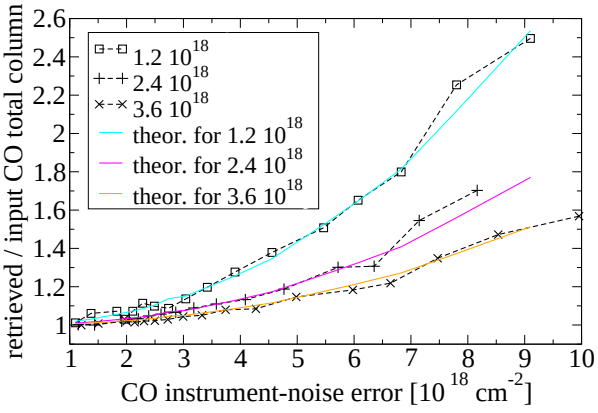

Fig. 4. Monte-Carlo calculations of the positive bias observed for CO as a function of the instrument-noise error for CO total columns of 1.2×10^{18} molec/cm^2, 2.4×10^{18} molec/cm^2, and 3.6×10^{18} molec/cm^2. (dashed lines). The corresponding theoretical curves (solid lines) based on numerical integration agree well with these calculations.

errors larger than 1.5×10^{18} molec/cm^{-2}. One reason for this positive bias is that the instrument noise itself has a Gaussian distribution, but the fitting is done in the $\ln(I/I_0)$ space and thus the instrument-noise error is related to the logarithm of the noise. In the case of large noise levels comparable with the actual absorption depth of the measured gas this results in a positive bias in the retrieved column for large instrument-noise errors. Figure 4 shows the size of this bias as a function of the instrument-noise error for different CO total columns based on Monte-Carlo calculations. The theoretical curves are based on a simplified model of one absorption line measured by one SCIAMACHY detector pixel. In reality, the SCIAMACHY spectra contain more than one CO absorption line which mostly cover more than one detector pixel and are often blended with other absorptions. However, the CO lines have comparable absorption depths and the best fit to the spectrum is determined by those lines falling onto detector pixels with the smallest noise levels, making it an acceptable simplification. Figure 4 clearly shows an increase in the bias with increasing instrument-noise error and the absolute value of the bias is almost independent of the CO column. The Monte Carlo simulations agree very well with what one would expect theoretically. The behaviour of the bias is similar to that found by de Laat et al. (2007), but the effect here is about 5 times smaller. Thus other effects contribute to the observed bias. The most likely candidates are calibration offsets which especially play a role for low signals which are correlated with large instrument-noise errors. Figure 5 shows the same Monte Carlo simulations as Fig. 4 but now with different calibration offsets added. It can be seen that the error in the applied orbital variation correction of $\sim$4$\pm$2 BU/s on average per detector pixel as found by Schrijver (2006) causes a significantly larger bias than without this additional offset, but it is still smaller than the observed bias. A fixed offset of $\sim$10 BU also introduces an instrument-noise error dependent bias. The size of the bias however depends on the nature of the applied offset: whether it is an offset which varies per detector pixel or a fixed offset over the whole wavelength range. The magnitude of the applied offsets in Fig. 5 are not unrealistic (see Sect. 3.2) and clearly demonstrate that further improvement of the SCIAMACHY calibration are likely leading to more accurate CO total columns for noise errors larger than $\sim1.5\times10^{18}$ molec/cm^2. Although de Laat et al. (2007) show that only about 10% of their data have such large noise errors they also note that these noise errors are especially found in regions with low surface albedos of $<$0.1, which corresponds to geographical regions where most of the CO surface emissions occur.

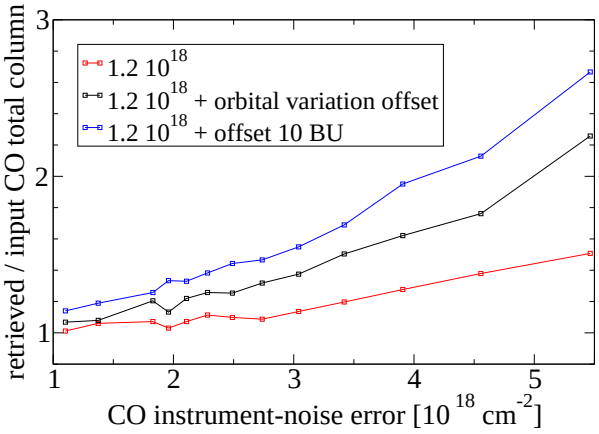

Fig. 5. As Fig. 4, but now including different calibration offsets in the simulations: no offset (red), an offset corresponding to the mean bias found for the orbital variation by Schrijver et al. (2006) of 4±2 BU/s (black), and a fixed offset of 10 BU (blue). Calculations are only done for a CO column of 1.2×10^{18} molec/cm^2.

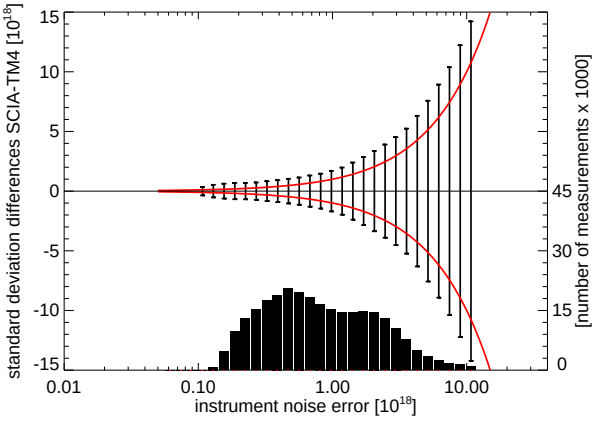

Fig. 6. Probability distribution of the standard deviation of the single SCIAMACHY-TM4 CH_4 total column differences as a function of instrument noise errors. The SCIAMACHY-TM4 differences are first binned according to their instrument-noise error, and then the standard deviation value is calculated for all differences within each instrument-noise error bin. The red line indicates the ($1\,\sigma$) error, whereas black lines indicate the standard deviation ($1\,\sigma$) of the differences. The black bars at the bottom of the graph indicate the total number of measurements with instrument-noise errors for each instrument-noise error bin. This graph is based on SCIAMACHY measurements for the year 2004 between 60° S and 60° N.

All results show that the bias is sufficiently small for instrument-noise errors smaller than $\sim1.5\times10^{18}$ molec/cm^2, justifying the exclusion of SCIAMACHY measurements with instrument-noise errors larger than this threshold by de Laat et al. (2007).

3.1.2 CH_4 instrument-noise error

Following the approach of de Laat et al. (2007) for CO, a similar statistical analysis can be performed for CH_4. Since CO and CH_4 are retrieved simultaneously, the same data set as in Gloudemans et al. (2006) and de Laat et al. (2007) is used, except that the selection criteria are different. For CH_4 only cloud-free measurements are taken into account, since Sect. 4.3 shows that clouds can have a significant impact on the retrieved CH_4 total columns. Figure 6 shows the standard deviation of the differences between single SCIAMACHY CH_4 total column measurements and the temporally and spatially collocated modeled CH_4 from the TM4 model. The TM4 model used is the same as in Gloudemans et al. (2006) and de Laat et al. (2007). For an ideal model simulation, and well-characterized measurements, the standard deviation of the differences should equal the corresponding instrument-noise error. Figure 6 shows that the standard deviation of the differences between SCIAMACHY CH_4 measurements and model results follow the instrument noise error level: the larger the noise error, the larger the standard deviation of the differences. The differences are mostly smaller than the $2\,\sigma$ instrument noise error. Only for small instrument-noise errors $<0.5\times10^{18}$ molec/cm^2 the standard deviation is somewhat larger and is relatively constant. However, such small noise errors only occur over bright surfaces, such as deserts, where aerosols may lead to a larger spread in the SCIAMACHY CH_4 total columns than calculated by the model (cf. Sect. 4.5).

Figure 7 shows the average difference between SCIAMACHY and modeled CH_4 total columns for each instrument-noise error interval. The differences are smaller than the $2\,\sigma$ instrument-noise error and follow closely the $1\,\sigma$ noise error up to noise errors of 2×10^{18} molec/cm^2. For larger noise errors the differences are relatively constant at a level of $\sim-2\times10^{18}$ molec/cm^2 which corresponds to $\sim$5% of the CH_4 total column.

CH_4 is a strong absorber with about 10 times deeper absorptions than those for CO. Therefore the theoretical bias as found for CO in Fig. 4 is much smaller for CH_4 and only gives biases larger than 1% for noise errors $>5\times10^{18}$ molec/cm^2. Also, this bias is positive and thus cannot explain the observed negative bias. Calibration offsets on the other hand can also produce biases in the retrieved CH_4 total columns. Figure 8 shows the equivalent of Fig. 5 but now for CH_4, based on the same Monte Carlo simulations as those for CO, since both molecules are retrieved simultaneously. It can be seen that a fixed offset of 10 BU results in a positive bias as is seen for CO and thus cannot explain the observed negative bias. Also, the size of the bias is much larger than observed. The error in the applied orbital variation of the dark signal which varies per detector pixel however results in a negative bias, which is almost independent of noise error. This is very similar to the observed bias, except that

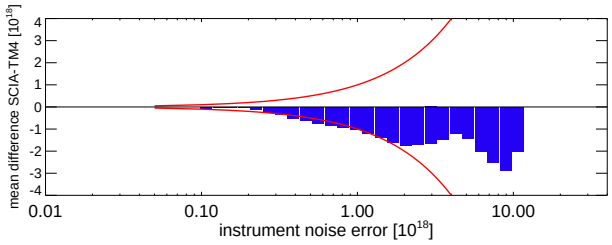

Fig. 7. Average differences (blue) between the SCIAMACHY and TM4 CH_4 total columns corresponding to Fig. 6. The red line indicates the 1σ instrument-noise error.

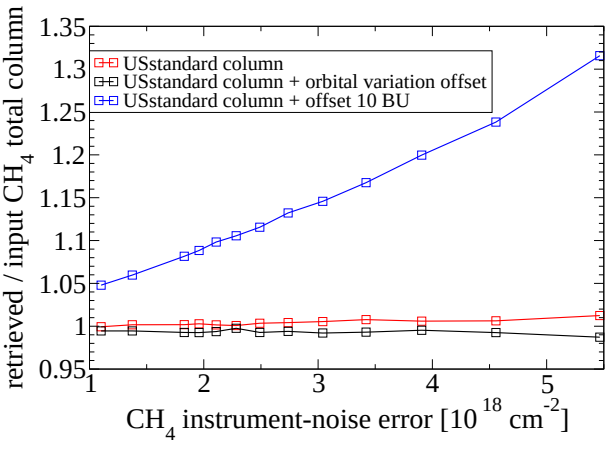

Fig. 8. As Fig. 5, but now for CH_4.

it is smaller than observed. Figure 8 and Fig. 5 suggest that a detector pixel dependent calibration error is more likely to explain the observed biases in CO and CH_4 than a fixed offset.

3.2 SCIAMACHY minor calibration issues

Although the most important SCIAMACHY calibration issues, i.e. the ice layer growing onto the near-infrared detectors, the variation of the dark signal within an orbit, and the increasing number of damaged detector pixels are solved and/or corrected for (cf. Gloudemans et al., 2005), some minor calibration issues remain. The empirical correction for the ice layer as described in Gloudemans et al. (2005) is not included in the instrument model, but since it resembles an additional wavelength-independent background signal for small enough retrieval windows it is included in the vector ***B*** in Eq. (8). Inaccuracies in this correction method typically cause errors in the retrieved CO and CH_4 total columns of ∼1–2%. This is well within the required precision and accuracy of the CO total columns of ∼10–20%, but a significant source of uncertainty for CH_4 retrieved from the 2.3 μm spectra. Section 3.1.2 shows that for CH_4 a bias of ∼5% is present, which is probably explained by a combination of uncertainties in the ice layer correction, a small theoretical bias, and calibration biases, the latter having the largest impact. This makes their quality less than that of the CH_4 total columns retrieved from the spectra around 1.6 μm (Schrijver et al., 2006; Frankenberg et al., 2006).

Besides the uncertainty in the ice layer correction, other calibration issues can still play a role. For example, the SCIAMACHY measured solar spectrum cannot be applied directly in the IMLM algorithm, since it contains instrument effects such as spectral dispersion and damaged or noisy detector pixels which would spoil the forward model. In order to account for these instrument effects, the high-resolution ATMOS spectrum has been fed into the instrument model to obtain a solar spectrum on the SCIAMACHY detector pixel grid (cf. Sect. 2.1.2). Comparison of this modeled SCIAMACHY solar spectrum with the specially calibrated SCIAMACHY solar reference spectrum (provided by J. Frerick, ESA) leads to a correction factor for each detector pixel which is included in the forward model as a vector multiplication of the term **PAI** in Eq. (8). Using daily measured SCIAMACHY solar spectra instead of the specially calibrated SCIAMACHY solar spectrum does not lead to improvements in the retrieved CO and CH_4 total columns.

SCIAMACHY's detectors show a deviation of the detector response from a chosen linear reference curve, the non-linearity. On average, the derived non-linearity correction for the 2.3 μm wavelength region constitutes less than 0.3% of the atmospheric signal after dark signal correction, both for low and high surface albedos. This has a negligible effect on the retrieved CO and CH_4 total columns and is therefore not taken into account in the IMLM retrievals of the SCIAMACHY spectra. However, the actual non-linearity varies per detector pixel and Figs. 5 and 8 show that detector-pixel dependent offsets may be responsible for the observed biases in the retrieved CO and CH_4 total columns for large instrument-noise errors. Similarly, the correction for the variation of the dark signal over the orbit in the SCIAMACHY retrievals (cf. Gloudemans et al., 2005) has an estimated uncertainty of ∼4±2 BU/s (Schrijver, 2006). For high surface albedo areas such as deserts, this has only a minor effect on the retrieved CO columns of less than ∼5%. However, for low surface albedos of ∼0.05 the uncertainty can easily constitute up to 4% of the atmospheric signal, which can lead to significant errors in the retrieved CO and CH_4 columns as is shown in Sect. 3.1. A better correction for the variation of the dark signal over the orbit and inclusion of a correction for the non-linearity is currently underway.

Finally, not for every orbit the corresponding dark signal is available. Especially shortly after a decontamination period, when the ice layer is growing fast and consequently the dark signal is decreasing rapidly, using the dark signal of a nearby orbit may result in systematic errors in the signal level of up to ∼25 BU/s. However, this concerns only a small fraction of the orbits and this error is generally less than ∼10 BU/s.

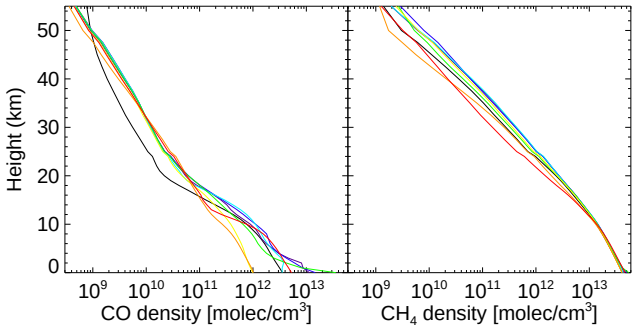

Fig. 9. The atmospheric CO (left) and CH_4 (right) vertical profiles used in the sensitivity study.

In summary, systematic errors in the measured SCIAMACHY signal around 2.3 μm should be reduced to within ~1 BU, or similarly ~1% of the atmospheric signal for low surface albedos after correction for all instrument effects, in order to have accurate CO and CH_4 retrievals over both high and low surface albedos. Further efforts are under way to meet this requirement as close as possible.

4 Simulated retrievals

As shown in Fig. 7, and additionally by de Laat et al. (2007), for small instrument-noise errors a small bias exists. Minor calibration problems may explain part of this bias as discussed in Sect. 3.2, but uncertainties in different retrieval parameters may also play a role. The effects of the most important uncertainties in the 2.3 μm region are discussed in the following subsections using simulated retrievals. These simulated retrievals use eight different trace gas profiles representing a wide range of CO and CH_4 vertical distributions including the US standard atmosphere profiles (see Fig. 9).

4.1 Total column averaging kernels

The IMLM retrieval algorithm has been developed to retrieve total columns from near-infrared nadir measurements, for which height-resolved information is very poor, implying that only one vertically resolved measurement is available. Therefore the IMLM method is based on scaling the a priori atmospheric trace gas profiles. Such an approach does not allow to calculate true averaging kernels, but instead total column averaging kernels, A_{TC}, have been computed for each trace gas k following the approach of Buchwitz et al. (2004):

$$A_{\mathrm{TC},k}(P_j) = (C_{\mathrm{rc},k} - C_{\mathrm{ac},k})/(C_{\mathrm{pc},k} - C_{\mathrm{ac},k}). \quad (15)$$

Here, P_j is the pressure of layer j of the a priori atmosphere used in the forward model described in Sect. 2.1.1 and C_{ac} the total column of the a priori trace gas profile, C_{pc} the total column of the perturbed profile which corresponds to an

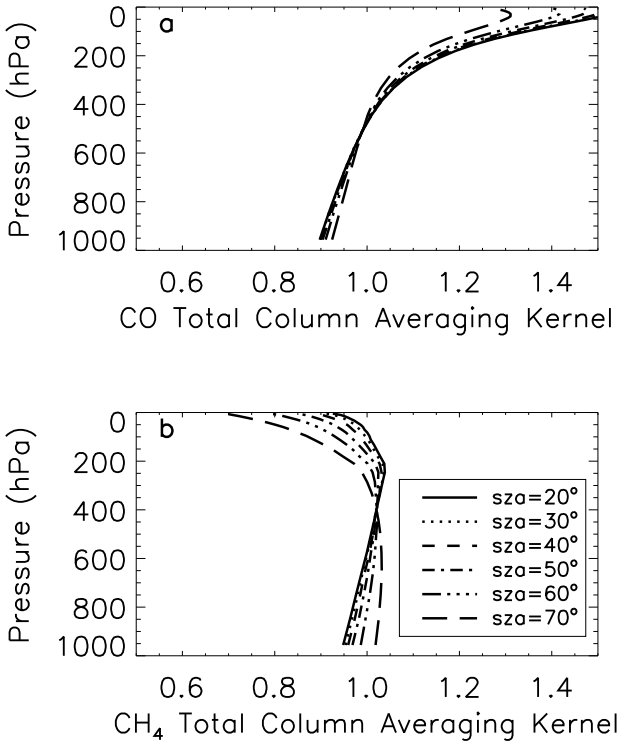

Fig. 10. The total column averaging kernels for IMLM retrievals of CO and CH_4 total columns from SCIAMACHY's channel 8. **(a)** CO **(b)** CH_4.

enhancement of the a priori profile in layer j, and C_{rc} is the corresponding retrieved total column. Total column averaging kernels have been calculated for the eight different trace gas profiles including the US standard atmosphere. The resulting total column averaging kernels do not show a strong dependence on the chosen atmospheric trace gas profile or the surface albedo. However they depend strongly on the solar zenith angle. Figure 10 shows the CO and CH_4 total column averaging kernels for the IMLM retrieval method in the 2.3 μm wavelength range. It can be seen that the total column averaging kernels for CO and CH_4 are close to 1 up to ~200 hPa, indicating that changes throughout the troposphere, where most of the CO and CH_4 is located, are well-captured. In the case of SCIAMACHY 2.3 μm nadir measurements the depencence on the viewing angle is negligible.

CO and CH_4 absorption lines become narrower and deeper when the temperature and pressure decrease, for constant trace gas columns (Fig. 11). In the Earth's atmosphere the amount of both CO and CH_4 however decreases rapidly with increasing altitude, so that the contribution of the bottom layers with the highest pressure levels to the total absorption depth is largest. Because of the lack of vertical resolution and by using the IMLM fitting procedure, which scales the a priori trace gas profiles as a whole, a perturbation at

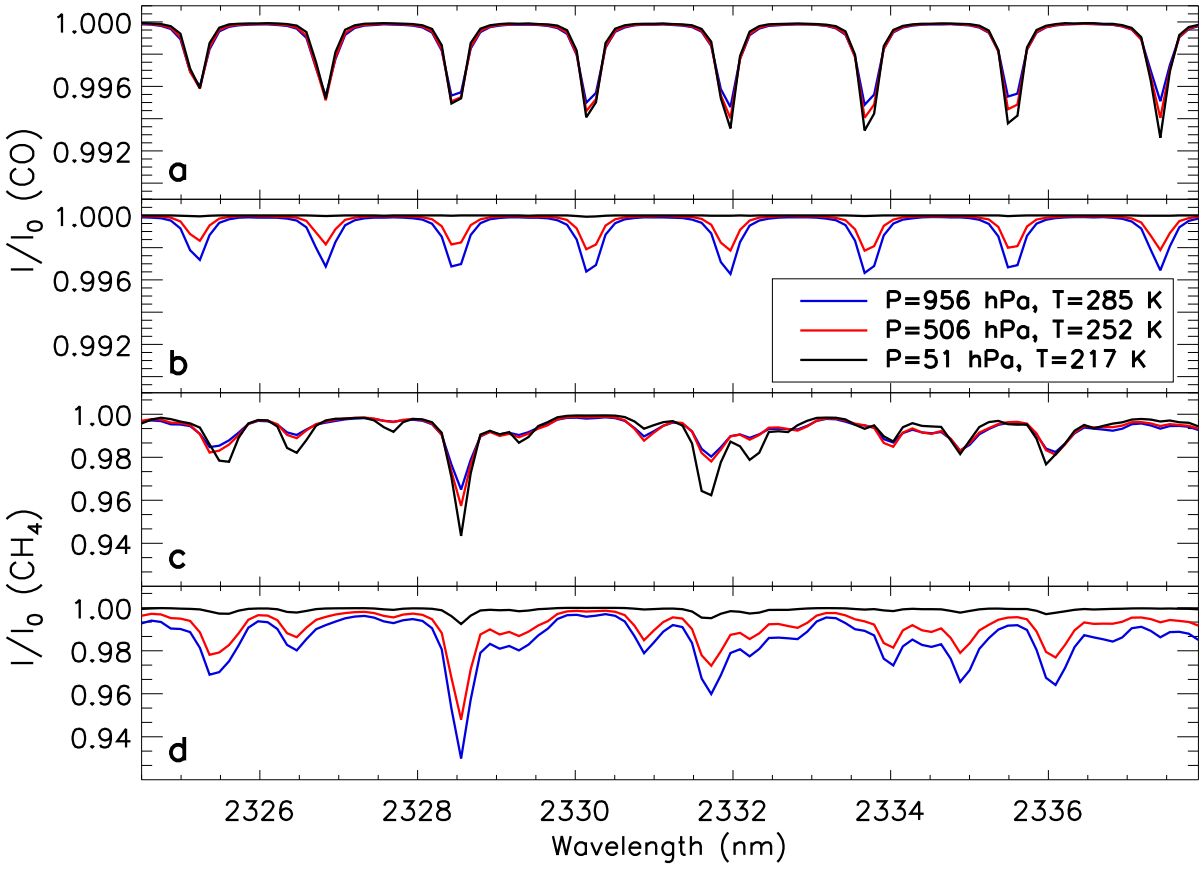

Fig. 11. Behaviour of the CO and CH_4 absorption lines in SCIAMACHY's channel 8 for temperature and pressure levels corresponding to different atmospheric layers of the US standard atmosphere. **(a)** CO absorption lines for a column density of 5×10^{17} molecules/cm^2. **(b)** As (a) but using the column densities of each corresponding layer of the US standard atmosphere, i.e. 3.6×10^{17} (blue), 1.9×10^{17} (red), and 2.2×10^{15} molecules/cm^2 (black). **(c)** As (a) but for CH_4 using a column density of 2×10^{18} molecules/cm^2. **(d)** As (b), but for CH_4. The column densities used are 4.1×10^{18} (blue), 2.5×10^{18} (red), and 2.4×10^{17} molecules/cm^2 (black).

low pressure levels is partially fitted as a larger perturbation at higher pressure levels. Since the CO lines are weak and well-separated this leads to an overestimation of the CO total columns for positive perturbations at altitudes above the ~200 hPa level and an underestimation for negative perturbations both resulting in $A_{\mathrm{TC}}>1$ (cf. Eq. 15). However, only a small fraction of the CO total column resides above ~200 hPa and doubling this amount causes an error in the retrieved CO total column of less than ~5%. MOPITT measurements at 150 and 250 hPa show that variations at these pressure levels are typically less than 100%. (cf. http://www.eos.ucar.edu/mopitt/data/plots/mapsv3_mon.html).

Although the temperature and pressure behaviour of the strongest CH_4 absorption lines is similar to those of CO, the wealth of CH_4 lines in the 2.3 μm region causes the appearance of a CH_4 continuum absorption for higher temperatures and pressure levels. This is caused by broadening of the often overlapping CH_4 lines at higher pressure levels and weaker CH_4 lines becoming more pronounced at higher temperatures. This causes the total column averaging kernels for CH_4 to show a different behaviour than those for CO. Figure 11 illustrates these effects for CO and CH_4.

Application of the total column averaging kernel for species k to a comparison data set is as follows:

$$C_{x_{\mathrm{comp},k}} = C_{\mathrm{ac},k} + A_{\mathrm{TC},k}(P_j)(x_{\mathrm{comp},k} - x_{\mathrm{ac},k}). \quad (16)$$

Here, $C_{\mathrm{ac},k}$ is the total column of the a priori trace gas profile for species k and $x_{\mathrm{ac},k}$ are its partial columns on the pressure grid P_j. $x_{\mathrm{comp},k}$ are the partial columns of the comparison data set on the pressure grid P_j and $C_{x_{\mathrm{comp},k}}$ are the resulting total columns of the comparison data set that can be compared with the total columns retrieved with the IMLM method.

When compared with other data sets application of the total column averaging kernel as in Eq. (16) eliminates errors from the comparison that are caused by a true profile that deviates from the a priori profile. For CO the IMLM retrievals are not very sensitive to the true CO vertical profile and

Table 1. Effect of using a fixed trace gas profile in the forward model on the retrieved CO and CH_4 total columns in percentages of the true total column. The results are valid for solar zenith angles between 10° and 70° and surface albedos between 0.05 and 0.6, and denote the maximum error found for these scenarios.

	CO columns			CH_4 columns		
Spectral range[a]:	*R*	*P*	*P*+*R*	*R*	*P*	*P*+*R*
CO profile	<7.5	<7.5	<7.0	<0.1	<0.2	<0.14
CH_4 profile	<0.4	<2.5	<0.8	<0.3	<0.75	<0.5

[a] Spectral ranges are chosen to include CO *R*-branch lines between 2324.5 and 2337.9 nm, CO *P*-branch lines between 2353.8 and 2370.0 nm, or both (2324.5–2370.0 nm). A multitude of CH_4 lines are present in all three spectral ranges.

the corresponding errors in the retrieved total columns are <7.5% which is well within the instrument-noise error of single SCIAMACHY CO measurements (de Laat et al., 2006, 2007). Thus for SCIAMACHY CO total column data the application of the total column averaging kernels is not very important. For CH_4 these errors are smaller than 0.75%. Table 1 shows that this error also depends on the chosen retrieval window: the errors for retrieval of CH_4 between 2353.8 and 2370.0 nm, covering the wavelength range of CO *P*-branch lines, is more than twice as large as for retrievals between 2324.5 and 2337.9 nm containing CO *R*-branch lines. The latter wavelength range corresponds to the retrieval window used by de Laat et al. (2006, 2007), and Gloudemans et al. (2006).

4.2 Temperature and water vapor

The current version of the IMLM retrieval method includes temperature and water vapour profiles from ECMWF data as a priori information. The reason for this is that the lack of a correct temperature profile can lead to significant errors in the retrieved trace gas columns as has already been pointed out by Buchwitz and Burrows (2004) and Frankenberg et al. (2005b). For the IMLM retrieval method these errors are typically less than 25% for CO and a few percent for CH_4. Thus, including temperature and water vapour profiles from ECMWF data is important for the near-infrared retrieval of CO and CH_4. Errors in the ECMWF temperature profiles of a few kelvin result in CO and CH_4 total column errors below 1%. The ECMWF water vapour profiles are less well-determined in regions of deep convection (Flentje et al., 2007) but even errors in the water vapour profile of up to ∼25% induce errors in the CO and CH_4 total columns of less than 1%.

A more important issue is the interference of strong H_2O absorptions with the much weaker CO absorption lines around 2.3 μm which are mostly comparable to the noise level of the SCIAMACHY spectra. Since including the strong H_2O lines in the retrieval generally leads to an underestimate of the CO total columns of $\sim 0.2\times10^{18}$ molec/cm^2, the strongest H_2O lines have been excluded from the fit.

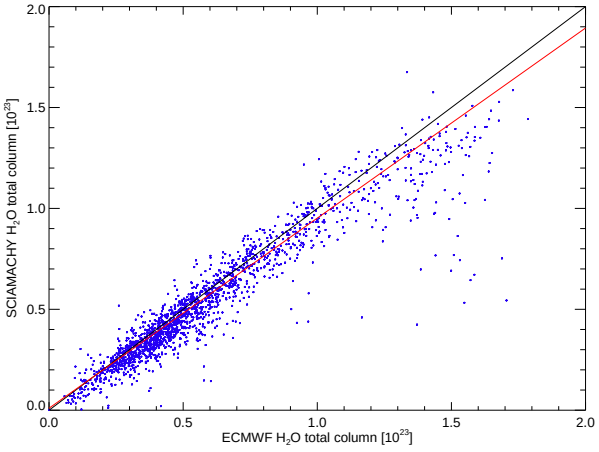

Fig. 12. Monthly mean SCIAMACHY H_2O total columns versus the spatially and temporally collocated ECMWF H_2O total columns for September 2003. Each data point represents the weighted average H_2O total column within a $3°\times2°$ grid box with the inverse square of the SCIAMACHY H_2O noise error used as the weight. The red line denotes the weighted linear least squares fit to all data points using the same weights. The slope of the fit is 0.94 and the offset is 0.01×10^{23} molec/cm^2. The correlation is 0.96 and the scatter is $\sim0.06\times10^{23}$ molec/cm^2. The black line denotes the expected 1:1 correlation. Other months give similar results.

The strong H_2O lines have a negligible effect on the CH_4 columns which have comparable absorption depths. Overlapping CH_4 absorptions do not appear to influence the retrieved CO total columns. Because of the overlapping H_2O, CO, and CH_4 lines, all three species have to be retrieved simultaneously. Therefore it is also important to know the quality of the H_2O total columns retrieved from the same spectra with the strongest absorptions being excluded from the fit. Figure 12 shows that in that case the SCIAMACHY H_2O total columns compare well with the spatially and temporally collocated H_2O total columns from ECMWF data. Figure 12 shows no significant bias between SCIAMACHY and ECMWF H_2O total columns, indicating that the quality

of the retrieved SCIAMACHY H_2O total columns is sufficient to avoid a dominant effect on the CO total columns retrieved from the same spectra.

4.3 A priori atmospheric profiles and surface pressure

Due to the overlapping CO and CH_4 absorption lines in the 2.3 μm region, deviations of the a priori profile from the true profile of one molecule can also influence the retrieval of another molecule, which is not accounted for by the total column averaging kernel when comparing to other data sets. In order to quantify this effect, typical scenarios observed with SCIAMACHY, i.e. surface albedos between 0.05 and 0.6 and solar zenith angles between 10° and 70° (de Laat et al., 2006, 2007) have been investigated. Table 1 shows that the CH_4 profile has a negligble effect of <2.5% on the retrieved CO total columns and the effect of the CO profile on the CH_4 total columns is <0.2%. It also shows that the effect of the CH_4 profile is about 6 times smaller for the 2324.5–2337.9 nm retrieval window compared to the 2353.8–2370.0 nm window which shows the maximum effect, and about 2 times smaller for the effect of the CO profile.

As pointed out by Frankenberg et al. (2005b) not taking into account the surface pressure in the a priori atmospheric profiles can introduce significant biases in the retrieved total columns. The IMLM method avoids these errors by using a priori trace gas and temperature profiles including surface pressure variations using for each SCIAMACHY ground pixel the corresponding ECMWF surface pressure. Errors in the CO and CH_4 total columns due to uncertainties in the ECMWF surface pressure are negligible.

Retrieval of CO and CH_4 total columns over clouded ground scenes have a similar effect, since in that case only the column above the cloud is retrieved and cloud top height is not taken into account in the a priori profiles used in the IMLM algorithm. For CH_4 the latter can introduce significant errors of a few percent in the partial CH_4 column above clouds with a cloud top height of up to 750 hPa. Therefore only cloud-free scenes have been analyzed up till now. CH_4 retrievals over clouded scenes will become more accurate if the cloud top height is included in the retrieval algorithm, but in that case one still has to account for the "missing part" of the total column below the cloud, which can be up to ∼25% of the total CH_4 column for clouds at 750 hPa. For CO, the effect of using an a priori profile starting at the surface pressure on the partial column above clouds up till 750 hPa is also a few percent for retrievals between 2324.5 and 2337.9 nm. In the case of SCIAMACHY, this is not significant since the instrument-noise errors of single CO measurements are much larger (de Laat et al., 2006, 2007). The "missing part" of the column below such clouds can however be a significant fraction of the CO total column, especially over source regions. Therefore, inclusion of completely clouded scenes as is done in Gloudemans et al. (2006) is acceptable for CO, but only when the "missing part" of the total column is small, which is the case for smoke/clouds close to the surface. In order to avoid significant negative biases due to missing a large part of the CO column below the cloud Gloudemans et al. (2006) first compared CO columns over clouded scenes with those over nearby cloud-free scenes before including the retrieved CO columns over clouded scenes in the analyses.

4.4 Spectroscopic parameters

Besides uncertainties in the atmospheric profiles, uncertainties in the spectroscopic parameters used can also introduce errors in the retrieved trace gas columns. The IMLM method uses the HITRAN 2004 database for the spectroscopic parameters which includes estimated uncertainty intervals for the line strength and line broadening parameters of each transition (Rothman et al., 2005). These uncertainties range from 2–5% for the strongest CH_4 transitions to >20% for the weakest CH_4 transitions. For the CO lines in the 2.3 μm region, the uncertainties in the intensities are 2–5% and within 2% for the line broadening parameters (Rothman et al., 2005). The corresponding errors in the retrieved total columns have been investigated by constructing synthetic measurements with either increased or decreased line intensities or broadening parameters and retrieving those with the HITRAN 2004 spectroscopic data base for each of the 8 different a priori atmospheres, solar zenith angles between 10° and 70°, and surface albedos between 0.05 and 0.6. For each transition, the upper limits of the uncertainty intervals have been used to calculate its increased and decreased intensities and line broadening parameters. For transitions with an estimated uncertainty of >20%, a 20% increase or decrease has been applied. Since this only concerns the weakest lines, these have only a minor impact on the retrieved column. The results are presented in Table 2. Since CH_4, CO, and H_2O lines overlap in the 2.3 μm wavelength range also the effect of the CH_4 spectroscopic parameters on the retrieved CO columns and vice versa are listed, as well as the effect of the H_2O parameters on both molecules. It can be seen that uncertainties in the CO line intensity and broadening have a negligible effect on the retrieved CO and CH_4 total columns. The effects of the uncertainties in the CH_4 and H_2O line parameters are <15% and thus also smaller than the current precision of the individual SCIAMACHY CO measurements (de Laat et al., 2006). The effect is significantly larger for the 2353.8–2370.0 nm and 2324.5–2370.0 nm retrieval windows compared to the 2324.5–2337.9 nm spectral range, except for the H_2O intensity. The effect of the H_2O broadening on the CO columns retrieved between 2353.8–2370.0 nm is reduced when the strongest H_2O lines are excluded from the fit (see also Sect. 4.2).

Uncertainties in the H_2O parameters do not have a significant effect on the retrieved CH_4 columns. As for CO, the effect of the H_2O broadening on the CH_4 columns retrieved between 2353.8–2370.0 nm is reduced when the strongest H_2O lines are excluded from the fit. The CH_4

Table 2. Effect of uncertainties in spectroscopic parameters on the retrieved trace gas columns. Absolute deviations from the true columns in percentages are listed for a solar zenith angle range of 10–70° and albedo range 0.05–0.6. The numbers are based on calculations using for each line the highest value of its associated error code range as given by the HITRAN database. The errors denote the maximum error found for these scenarios.

	CO columns			CH_4 columns		
Spectral range[a]:	*R*	*P*	*P*+*R*	*R*	*P*	*P*+*R*
CO intensity	<2–5[b]	<2–5[b]	<2–5[b]	<0.007	<0.004	<0.004
CO broadening	<0.4	<0.4	<0.4	<0.01	<0.01	<0.005
CH_4 intensity	<0.9	<9	<7	<2–5[c]	<2–5[c]	<2–5[c]
CH_4 broadening	<3	<12	<14	<0.7	<3	<1.5
H_2O intensity	<0.2	<0.1	<0.1	<0.01	<0.004	<0.02
H_2O broadening	<2	<15	<5	<0.6	<1.3	<0.6

[a] Spectral ranges are chosen to include CO *R*-branch lines between 2324.5 and 2337.9 nm, CO *P*-branch lines between 2353.8 and 2370.0 nm, or both (2324.5–2370.0 nm). A multitude of CH_4 lines are present in all three spectral ranges.
[b] The HITRAN database lists an uncertainty in the CO line intensities of 2–5% which translates directly into an uncertainty of the retrieved CO columns of the same order.
[c] The HITRAN database lists an uncertainty in the strongest CH_4 line intensities in the 2.3 μm region of 2–5% which translates directly into an uncertainty of the retrieved CH_4 columns of the same order.

broadening parameters also have a small effect on the retrieved CH_4 columns, although the effect in the 2353.8–2370.0 nm and 2324.5–2370.0 nm ranges is clearly larger than in the 2324.5–2337.9 nm spectral range. Especially the effect of the broadening in the 2353.8–2370.0 nm retrieval window is close to the current precision of the CH_4 retrievals and thus may play an important role. Uncertainties in the CH_4 line intensities have a significant effect on the CH_4 total columns of ∼2–5% depending on how accurate the uncertainty estimates of the HITRAN database are (Table 2). On average, the uncertainties in the line intensities for the strongest unblended transitions are ∼3% (L. Brown, private communication, 2007).

In the case of SCIAMACHY measurements in the 2.3 μm region, the empirical correction for the ice layer is based on calibrating the CH_4 total columns over the Sahara to model values (Gloudemans et al., 2005). This implies that this empirical correction for SCIAMACHY measurements around 2.3 μm may also partially compensate for uncertainties in the CH_4 spectroscopic parameters. In order to discriminate between ice layer and spectroscopic effects, more accurate spectroscopic parameters for the CH_4 octad bands in the 2.3 μm region are required. This is also important for future instrumentation measuring in the 2.3 μm wavelength range with similar spectral resolution as SCIAMACHY.

Other spectroscopic uncertainties in e.g., the coefficient of the temperature dependence of the line broadening, result in errors in the retrieved CO and CH_4 total columns of less than 0.4% for CO and less than 0.1% for CH_4 and thus are negligble compared to other error sources.

4.5 Scattering effects

Scattering in the atmosphere is not included in the forward model. To study the effect of Rayleigh and aerosol scattering on the retrieved CO and CH_4 total columns, the retrieval algorithm has been applied to synthetic measurements including these effects. The synthetic measurements have been calculated using the full line-by-line radiative transfer code from Hasekamp and Landgraf (2002, 2005) which includes Rayleigh and Mie (multiple) scattering. The line-by-line calculation of the optical depths follows the same procedure as in the retrieval algorithm. The above approach is similar to that in Houweling et al. (2005) and Aben et al. (2007), except that it is now applied to the 2.3 μm wavelength region including CO and CH_4 absorption lines. Four different aerosol types have been investigated. The aerosol size distribution of these aerosols and their scattering properties have been taken from Torres et al. (2001) and are summarized in Table 3.

The results show that Rayleigh scattering in this wavelength range has a negligible effect of <0.15% on the CO and CH_4 total columns. The effects of aerosol scattering depend on the vertical distribution of the aerosols, aerosol type, viewing geometry, and the underlying surface albedo. For marine and industrial aerosols most particles are located in the boundary layer and therefore a uniform distribution has been assumed up to 1 km, with an exponential decay above 1 km. In the case of biomass and mineral dust aerosols the particles can extend to much higher altitudes and also plumes of aerosols at a few kilometers altitude occur. For these aerosols three additional distributions have been investigated: extending the uniform distribution up to 3 and 5 km,

Table 3. Aerosol size distribution and scattering properties.

	Industrial	Biomass	Mineral dust	Marine
$Rm_{2.3}$	1.390	1.436	1.215	1.324
$Im_{2.3}$	-2.10×10^{-2}	-5.77×10^{-2}	-2.84×10^{-3}	-1.03×10^{-2}
$Rm_{0.55}$	1.473	1.529	1.530	1.381
$Im_{0.55}$	-5.00×10^{-3}	-2.68×10^{-2}	-5.50×10^{-3}	-3.70×10^{-9}
		Fine mode		
r_{eff}	0.117	0.197	0.105	0.105
v_{eff}	0.178	0.203	0.323	0.651
		Coarse mode		
r_{eff}	2.189	3.420	1.605	0.840
v_{eff}	0.810	0.866	0.418	0.651
Fraction	0.436×10^{-3}	0.294×10^{-3}	0.435×10^{-2}	0.153×10^{-1}

Rm_x,Im_x: real and imaginary part of the refractive index at "x" μm. r_{eff},v_{eff}: effective radius and variance of the size distribution in μm. Fraction: fractional contribution of the coarse mode to the number concentration.

respectively, with an exponential decay above these altitudes, and a plume of uniform density between 3 and 5 km altitude. The results for each of the four different aerosol types are discussed below.

4.5.1 Marine aerosols

The effects of marine aerosols are not important for SCIAMACHY 2.3 μm retrievals since the signal-to-noise ratio of these spectra over the ocean is too low due to the low surface albedo of <0.005. Also, the large SCIAMACHY footprint at 2.3 μm of 120 by 30 km includes only a small fraction of coastal area, where marine aerosols may be present. It should be noted however that for future satellite instruments with smaller satellite footprints and higher signal-to-noise ratios over the oceans, the effect of marine aerosols may no longer be negligible. Web-based images from the Multi-angle Imaging Spectrometer (MISR) (Kahn et al., 2005) indicate that the aerosol optical thickness (AOT) at 550 nm is seldom larger than 0.5 over the oceans or in coastal regions (http://eosweb.larc.nasa.gov/PRODOCS/misr/level3/level3_CGAS_small.html) and is usually below 0.3. The above calculations for the IMLM algorithm indicate for such AOTs an effect of <5% for CO and up to 2% for CH_4 over regions with surface albedos between 0.05 and 0.6, which can be a significant error source for CH_4 but not for CO. Including aerosol information in the retrieval algorithm can however significantly reduce this error (cf. Sect. 4.5.5).

4.5.2 Industrial aerosols

The results for industrial aerosols are shown in Fig. 13. For CO the effect is <5%, well within the current precision of the individual SCIAMACHY CO measurements (de Laat et al., 2007). For CH_4 effects up to 4% can be seen, but only for very high AOT values of ∼1 and solar zenith angles larger than 60°. The MISR images show that the AOT is usually less than 0.3 over such regions, corresponding to errors in the retrieved CH_4 columns of <1.5%, which is within the current precision of the SCIAMACHY CH_4 retrievals (see Sect. 3.1.2 and Schrijver et al., 2006). Also Edwards et al. (2004) show that in industrialized regions such as the eastern United States and western Europe the aerosol optical depth measured with the Moderate-Resolution Imaging Spectroradiometer (MODIS) has a maximum between April and August with AOTs <0.4. In the case of SCIAMACHY this corresponds to small errors in the CH_4 and CO total columns of <1% over these regions. Over heavily polluted China, MISR images indicate AOTs of up to ∼1 in some regions in March and October. This corresponds with errors of up to ∼2% for CH_4 for typical surface albedos of 0.05–0.1 and solar zenith angles of 20°–50° found over China. In these specific cases neglecting aerosol scattering in the retrieval algorithm may lead to significant errors in the retrieved CH_4 total columns.

4.5.3 Biomass aerosols

Biomass burning produces large quantities of aerosols, which can be uplifted to higher altitudes than 1 km and may be transported away from the source at higher altitudes (e.g. Bertschi and Jaffe, 2005; Tie et al., 2005). Figure 14 shows the effects of biomass aerosols on the retrieved CO and CH_4 columns for typical tropical biomass-burning conditions as observed by SCIAMACHY, i.e. a solar zenith angle of 30° and different vertical aerosol distributions. Over biomass-burning areas the aerosol optical depth can be up to 2, but decreases relatively fast away from the source (Edwards et al., 2006). MISR images suggest that the AOT is well below 1 in biomass-burning plumes. For CO, the effect of biomass

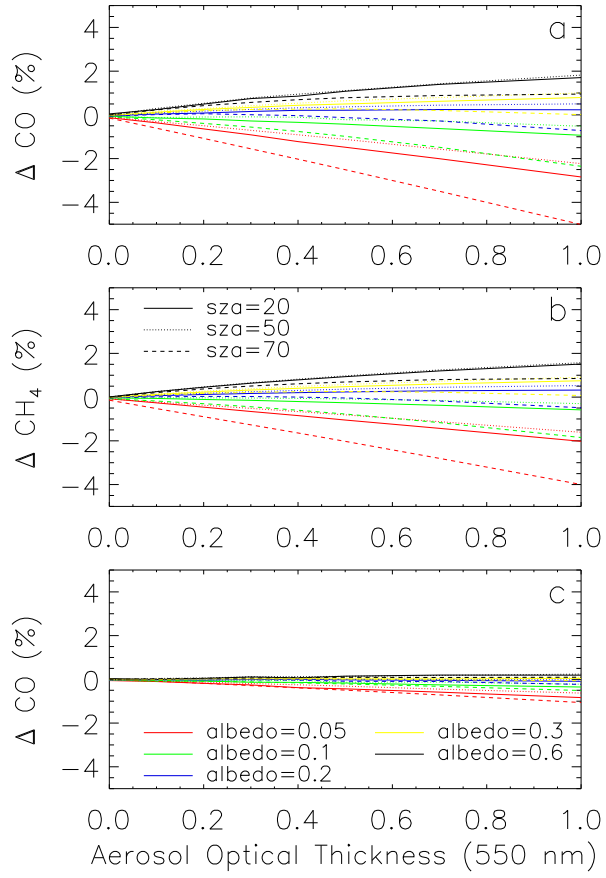

Fig. 13. Effect of industrial aerosols for different surface albedos and solar zenith angles (sza) on **(a)** CO, **(b)** CH_4, and **(c)** CO/CH_4 ratio multiplied with the true CH_4 column. The effect is expressed as the deviation from the true column.

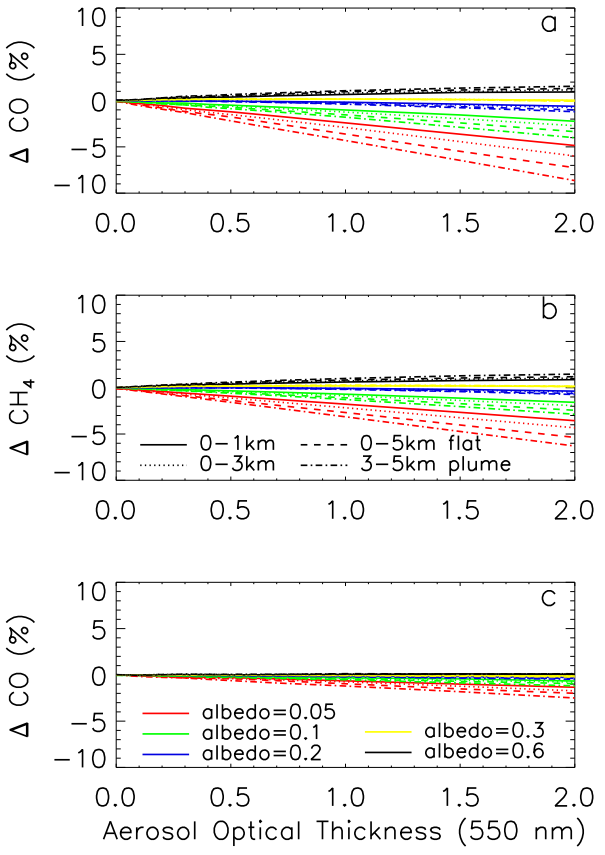

Fig. 14. Effect of biomass aerosols for a solar zenith angle of 30° for different surface albedos and vertical distributions. The effect on **(a)** CO, **(b)** CH_4, and **(c)** CO/CH_4 ratio multiplied with the true CH_4 column is shown, expressed as the deviation from the true column. Four different vertical aerosol distributions are shown: three distributions with a uniform layer up to 1 (solid line), 3 (dotted line), or 5 km (dashed line) with exponential decay above the uniform layer and one distribution with a single uniform layer between 3 and 5 km only (dot-dashed line) simulating an aerosol plume.

aerosols is <7% near source areas and well below 5% for biomass-burning plumes. For CH_4, effects of up to 5% can be found near biomass-burning sources, but are well below 3% in plumes. The effects on CO and CH_4 over the Northern Hemisphere forest fires in local summer are somewhat larger: <9% and <7% for CO and CH_4 respectively over source regions and <5% and <4% for CO and CH_4 in plumes. Thus only for CH_4 neglecting aerosol scattering in the retrieval algorithm may lead to significant errors in the retrieved total columns in regions with high loads of biomass aerosols.

4.5.4 Mineral dust aerosols

Dust storms over the Sahara can produce huge amounts of mineral dust aerosol up to about 5 km in summer that are also transported horizontally, creating plumes with higher aerosol loads at a few kilometers altitude and lower loads in the boundary layer (Karyampudi et al., 1999; de Reus et al., 2000; Haywood et al., 2003). Figure 15 shows the effect of mineral dust aerosols on the CO and CH_4 total columns for a solar zenith angle of 30°, corresponding to typical SCIAMACHY observations over desert areas. Aerosol optical depths of up to 2 are not uncommon in summer over the Sahara, but larger values are rare (Houweling et al., 2005). Figure 15 shows that the effect on the CO and CH_4 total columns may be as high as 10% during strong dust storms over the Sahara where the surface albedo can be up to ∼0.6 at 2.3 μm. Indeed clear correlations of enhanced SCIAMACHY CH_4 columns with aerosols are found over the Sahara in July 2004, with CH_4 total columns about 6% higher than both model calculations and the corresponding SCIAMACHY CH_4 measurements around 1.6 μm, which are corrected for aerosol effects by dividing them by the corresponding CO_2 columns from the same wavelength range (Schrijver et al., 2006; Frankenberg et al., 2006).

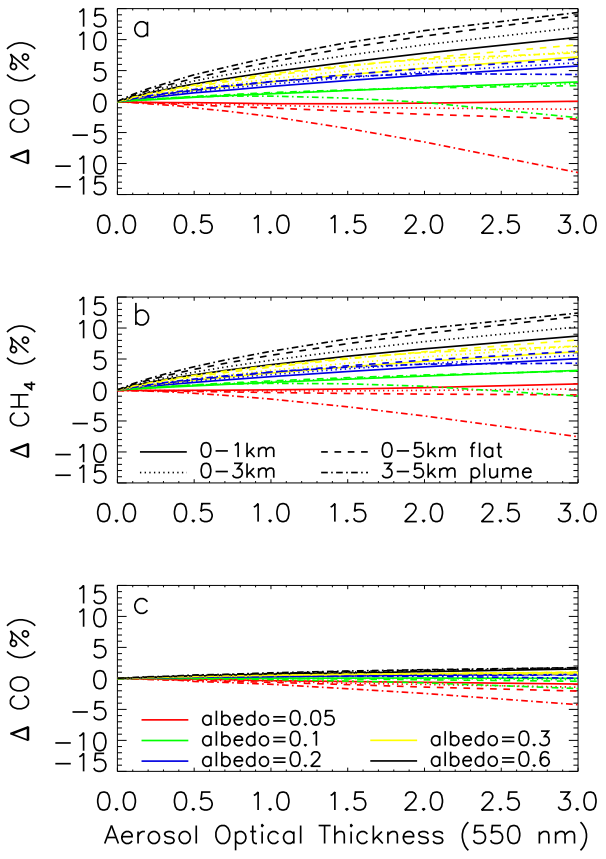

Fig. 15. As Fig. 14 but for mineral dust aerosols.

As noted in Gloudemans et al. (2005), the correction of the SCIAMACHY 2.3 μm spectra for the ice layer forming on the detector is based on CH_4 total columns over the Sahara. Spectra affected by dust aerosols lead to up to ∼3% lower correction values than non-affected spectra on the same day and these values have been excluded from the determination of the time-dependent ice layer correction. Thus the impact of mineral dust aerosols on the ice layer correction is kept as low as possible.

4.5.5 Summary aerosol scattering

It should be noted that the effects shown in Figs. 13, 14, and 15 purely demonstrate the effect on the retrieved total columns when no aerosol information is included in the retrieval. Clearly a simple first error correction using an aerosol climatology in the retrievals reduces these errors significantly. In addition the effect of aerosols on the retrieved columns is very similar for CO and CH_4. Since variations in the CH_4 total column are typically ±2% which is much smaller than the CO variability, and both molecules are retrieved simultaneously, this implies that using CH_4 as a proxy for the aerosol scattering effect on CO may also reduce the errors in the CO total columns. A similar approach has been successfully applied by Frankenberg et al. (2005a, 2006) for CH_4 retrievals in the 1.6 μm wavelength range. The retrieved CO/CH_4 total column ratio for the different aerosol scenarios has been calculated and multiplied with the true CH_4 total column in order to obtain a scaled CO total column. These results are shown in the bottom panels of Figs. 13, 14, and 15. The deviation of this scaled CO total column from the true CO total column is significantly smaller for large aerosol optical depths than in the case of using the retrieved unscaled CO total columns. For small AOTs the improvements become comparable to the variability in the CH_4 total columns and scaling of the CO total columns may introduce additional error sources. In these cases the unscaled CO total column is preferred. For marine aerosols similar results are obtained.

The results for the different aerosol types show that aerosols occuring over low surface albedo regions, such as industrial and biomass aerosols, lead to an underestimate of the CO and CH_4 columns. Over such regions, most of the light is absorbed by the surface and the contribution of photons scattered back from the aerosol layer is relatively high, reducing the effective optical path length. Larger AOTs and vertical distributions extending to larger altitudes further reduce the optical path length and thus the retrieved columns. On the other hand, aerosols over bright surfaces, such as mineral dust aerosols over deserts, overestimate the total columns. Here, most of the photons are reflected by the surface and are subsequently scattered in the aerosol layer, thus enhancing the effective optical path length. Larger AOTs and vertical distributions extending to larger altitudes further increase the optical pathlength, leading to an overestimate of the retrieved columns.

Mineral dust has the largest impact on the CO and CH_4 total columns retrieved from the 2.3 μm spectra. For CO retrieved from SCIAMACHY spectra this is generally not a significant effect, since the precision of single CO measurements is worse. Only in severe dust storms over the Sahara it may start playing a role for single measurements. In the case of SCIAMACHY measurements, these specific cases can be avoided by using the SCIAMACHY Aerosol Absorbing Index which detects UV absorbing aerosols including mineral dust and biomass aerosols (de Graaf et al., 2007). Also, using the retrieved CO/CH_4 column ratio significantly reduces the effect of ignoring aerosols in the retrieval algorithm over such regions. For CH_4 the effects on the total column are within ∼2–3% for most aerosol types which is around the current precision of the SCIAMACHY CH_4 measurements, but the effects for mineral dust may be substantially larger. For future instrumentation with better precision of single measurements than SCIAMACHY, aerosol effects may become an important issue for CH_4 over regions where the aerosol loads are high. However, including an aerosol climatology in the retrieval algorithm, using aerosol information from other spectral regions of the same instrument

such as the oxygen A-band, or from measurements by other satellite instruments, or, possibly, using a proxy for CH_4 may significantly reduce the errors shown here. This shows that aerosols are not a major error source for CO and CH_4 total column retrievals from either SCIAMACHY or future satellite instrumentation.

The results shown in Figs. 13, 14, and 15 are for the retrievals between 2324.5 and 2337.9 nm, but retrievals in other wavelength regions around 2.3 μm, e.g. between 2353.8 and 2370.0 nm or 2324.5–2370.0 nm do not differ significantly.

The IMLM algorithm does not include surface polarization and the polarization sensitivity of the satellite instrument in the forward model. In order to test the effect of polarization on the retrieved total columns synthetic measurements have been calculated with the same code used for the aerosol calculations in this section, but also including the surface polarization model from Rondeaux and Herman (1991) as well as the SCIAMACHY polarization sensitivity (Lichtenberg et al., 2005). The SCIAMACHY polarization sensitivity for the 2.3 μm wavelength range shows a weak and almost linear dependence on wavelength. The results show that for the SCIAMACHY instrument surface polarization has a negligible effect of $<$1% on the retrieved CO and CH_4 total columns in the 2.3 μm wavelength range.

5 Conclusions

The IMLM retrieval algorithm and its sensitivity to various retrieval parameters have been discussed. Application to SCIAMACHY 2.3 μm spectra shows that the major calibration issues are adequately solved and only minor issues remain. The dominant remaining error source for SCIAMACHY 2.3 μm spectra is the instrument-noise error. Errors due to uncertainties in retrieval parameters discussed in this paper are generally much smaller and mostly within the requirements for CO and CH_4 total columns. An explanation is given for the bias in the CO total columns seen by de Laat et al. (2007) for very large instrument-noise errors $>1.5\times10^{18}$ molec/cm^2 as well as for the bias in the CH_4 total columns, and an improved calibration will help to further reduce these biases. Specific conclusions are as follows:

- The positive bias for CO for SCIAMACHY instrument-noise errors larger than $\sim1.5\times10^{18}$ molec/cm^2 as found by de Laat et al. (2007) is partly due to a theoretical bias, but remaining calibration errors probably also contribute significantly. These errors are more important for low signals, but are negligible for instrument noise errors $<1.5\times10^{18}$ molec/cm^2.
- The CH_4 total columns from the SCIAMACHY 2.3 μm spectra agree well with TM4 model values. Only for instrument-noise errors larger than $\sim2\times10^{18}$ molec/cm^2 an almost constant negative bias of $\sim$5% is found. As for CO, this bias is most likely a combination of the theoretical bias and a bias due to calibration uncertainties. Efforts are under way to improve the current SCIAMACHY calibration in order to reduce the biases for large instrument-noise errors or equivalently low signals.
- The total column averaging kernels for CO and CH_4 are close to 1 up to $\sim$200 hPa, indicating good sensitivity throughout the troposphere.
- The use of a fixed a priori CO and CH_4 vertical profile has a negligible effect on the retrieved total columns. Errors due to uncertainties in the ECMWF temperature and water vapour profile, and the ECMWF surface pressure are also negligible.
- The retrieved H_2O total columns agree well with the corresponding ECMWF H_2O total columns.
- The sensitivity results for different microwindows around 2.3 μm indicate that in general the errors are smaller between 2324.5 and 2337.9 nm than in the 2353.8–2370.0 nm spectral range. Hence the IMLM retrieval method for the SCIAMACHY spectra has been applied to the 2324.5 and 2337.9 nm spectral range (de Laat et al., 2006; Gloudemans et al., 2006; de Laat et al., 2007).
- For the SCIAMACHY microwindow, the CH_4 intrinsic line intensity is the only spectroscopic parameter that introduces significant errors in the retrieved total columns and only for CH_4. It is important to better characterize the uncertainties in the HITRAN line intensities for CH_4 in order to better assess the impact on the CH_4 total columns from the 2.3 μm spectra and thus the need for more accurate CH_4 line intensities.
- Severe desert dust storms have the largest effect on the CO and CH_4 total columns due to scattering by aerosols and can lead to significant errors in the CH_4 total columns when no aerosol information is included in the retrieval algorithm. Plumes of biomass-burning aerosols can also have a significant effect on the retrieved CH_4 total columns, although these effects are smaller than for mineral dust. Using CH_4 as a proxy for CO and/or including aerosol information in the retrieval algorithm reduces these errors for both CO and CH_4 significantly.
- Polarization sensitivity of the SCIAMACHY instrument has a negligible effect of $<$1% on the retrieved CO and CH_4 total columns.

Acknowledgements. SCIAMACHY is a joint project of the German Space Agency DLR and the Dutch Space Agency NIVR with contribution of the Belgian Space Agency. We thank the Netherlands SCIAMACHY Data Center and ESA for providing data. The work performed is (partly) financed by NIVR. The authors thank

Jos de Laat, Christian Frankenberg, Sander Houweling, Ralph Snel, Rienk Jongma, and Linda Brown for useful discussions, and Jan Fokke Meirink for providing the TM4 CH_4 total column data. They also thank Arjo Segers, Coen Schrijvers, and Olaf Tuinder for providing the ECMWF data.

Edited by: A. Hofzumahaus

References

Aben, I., Hasekamp, O., and Hartmann, W.: Uncertainties in the space-based measurements of CO_2 columns due to scattering in the Earth's atmosphere, J. Quant. Spectrosc. Radiat. Trans., 104(3), 450–459, 2007

Anderson, G. P., Clough, S. A., Kneizys, F. X., Chetwynd, J. H., and Shettle, E. P.: AFGL Atmospheric Constituent Profiles (0–120 km), AFGL-TR-86-0110, Air Force Geophys. Lab., Hanscom AFB, Mass., 1986.

Bertschi I. T. and Jaffe, D. A.: Long-range transport of ozone, carbon monoxide, and aerosols to the NE Pacific troposphere during the summer of 2003: Observations of smoke plumes from Asian boreal fires, J. Geophys. Res., 110, D05303, doi:10.1029/2004JD005135, 2005.

Bovensmann, H., Burrows, J. P., Buchwitz, M., Frerick, J., Noël, S., Rozanov, V. V., Chance, K. V., and Goede, A.: SCIAMACHY: Mission Objectives and Measurement Modes, J. Atmos. Sci., 56, 127–150, 1999.

Buchwitz, M., Rozanov, V. V., and Burrows, J. P.: A near-infrared optimized DOAS method for the fast global retrieval of atmospheric CH_4, CO, CO_2, H_2O, and N_2O total column amounts from SCIAMACHY Envisat-1 nadir radiances, J. Geophys. Res., 105, 15 231–15 245, 2000.

Buchwitz, M. and Burrows, J. P.: Retrieval of CH_4, CO, and CO_2 total column amounts from SCIAMACHY near-infrared nadir spectra: Retrieval algorithm and first results, in Remote Sensing of Clouds and the Atmosphere VIII, edited by: Schäfer, K. P., Comèron, A., Carleer, M. R., and Picard R. H., Proceedings of SPIE, 5235, 375–388, 2004.

Buchwitz, M., de Beek, R., Bramstedt, K., et al.: Global carbon monoxide as retrieved from SCIAMACHY by WFM-DOAS, Atmos. Chem. Phys., 4, 1945–1960, 2004a, http://www.atmos-chem-phys.net/4/1945/2004/.

de Graaf, M., Stammes, P., and Aben, E. A. A.: Analysis of reflectance spectra of UV-absorbing aerosol scenes measured by SCIAMACHY, J. Geophys. Res., 112, D02206, doi:10.1029/2006JD007249, 2007.

De Laat, A. T. J., Gloudemans, A. M. S., Schrijver, H., van den Broek, M. M. P., Meirink, J. F., Aben, I., and Krol, M.: Quantitative analysis of SCIAMACHY carbon monoxide total column measurements, Geophys. Res. Lett., 33, L07807, doi:10.1029/2005GL025530, 2006.

De Laat, A. T. J., Gloudemans, A. M. S., Aben, I., Krol, M., Meirink, J. F., van der Werf, G. R., and Schrijver, H.: SCIAMACHY carbon monoxide total columns: statistical evaluation and comparison with CTM results, J. Geophys. Res., 112, D12310, doi:10.1029/2006JD008256, 2007.

de Reus, M., Dentener, F. J., Thomas, A., Borrmann, S., Ström, J., and Lelieveld, J.: Airborne observations of dust aerosol over the North Atlantic Ocean during ACE 2: Indications for heterogeneous ozone destruction, J. Geophys. Res., 105, 15 263–15 275, 2000.

Dils, B., De Mazière, M., Müller, J. F., et al.: Comparisons between SCIAMACHY and ground-based FTIR data for total columns of CO, CH_4, CO_2 and N_2O, Atmos. Chem. Phys., 6, 1953–1976, 2006, http://www.atmos-chem-phys.net/6/1953/2006/.

Edwards, D. P., Emmons, L. K., Hauglustaine, D. A., et al.: Observations of Carbon Monoxide and Aerosol From the Terra Satellite: Northern Hemisphere Variability, J. Geophys. Res., 109, D24202, doi:10.1029/2004JD0047272004, 2004.

Edwards D. P., Emmons, L. K., Gille, J. C., et al.: Satellite-observed pollution from Southern Hemisphere biomass burning, J. Geophys. Res., 111, D14312, doi:10.1029/2005JD006655, 2006.

Ehret, G. and Kiemle, C.: Requirements Definition for Future DIAL Instruments, Final Report, ESA R FQ reference: IMT-CSO/FF/fe/03.887; RFQ/3-10880/03/NL/FF, DLR reference: 3 472 749, DLR, 2005.

Flentje, H., Dörnbrack, A., Fix, A., Ehret, G., and Hólm, E.: Evaluation of ECMWF water vapour analyses by airborne differential absorption lidar measurements: a case study between Brasil and Europe, Atmos. Chem. Phys., 7, 5033–5042, 2007, http://www.atmos-chem-phys.net/7/5033/2007/.

Frankenberg, C., Meirink, J. F., van Weele, M., Platt, U., and Wagner, T.: Assessing Methane Emissions from Global Space-Borne Observations, Science, 308, 1010–1014, doi:10.1126/science.1106644, 13 May 2005, Science Express 17 March 2005, 2005a.

Frankenberg, C., Platt, U., and Wagner, T.: Iterative maximum a posteriori (IMAP)-DOAS for retrieval of strongly absorbing trace gases: Model studies for CH_4 and CO_2 retrieval from near infrared spectra of SCIAMACHY onboard ENVISAT, Atmos. Chem. Phys., 5, 9–22, 2005b, http://www.atmos-chem-phys.net/5/9/2005/.

Frankenberg, C., Meirink, J. F., Bergamaschi, P., Goede, A. P. H., Heimann, M., Körner, S., Platt, U., van Weele, M., and Wagner, T.: Satellite chartography of atmospheric methane from SCIAMACHY on board ENVISAT: Analysis of the years 2003 and 2004, J. Geophys. Res., 111, D07303, doi:10.1029/2005JD006235, 2006.

Gloudemans, A. M. S., Schrijver, H., Kleipool, Q., et al.: The impact of SCIAMACHY near-infrared instrument calibration on CH_4 and CO total columns, Atmos. Chem. Phys., 5, 2369–2383, 2005, http://www.atmos-chem-phys.net/5/2369/2005/.

Gloudemans, A. M. S., Krol, M. C., Meirink, J. F., de Laat, A. T. J., van der Werf, G. R., Schrijver, H., van den Broek, M. M. P., and Aben, I.: Evidence for long-range transport of Carbon Monoxide in the Southern Hemisphere from SCIAMACHY observations, Geophys. Res. Lett., 33, L16807, doi:10.1029/2006GL026804, 2006.

Hasekamp, O. P. and Landgraf, J.: A linearized vector radiative transfer model for atmospheric trace gas retrieval, J. Quant. Spectrosc. Radiat. Trans., 75, 221–238, 2002.

Hasekamp, O. P. and Landgraf, J.: Linearization of vector radiative transfer with respect to aerosol properties and its use in remote sensing, J. Geophys. Res., 110, D04203, doi:10.1029/2004JD005260, 2005.

Haywood, J., Francis, P., Osborne, S., Glew, M., Loeb, N., High-

wood, E., Tanre, D., Myhre, G., Formenti, P., and Hirst, E.: Radiative properties and direct radiative effect of Saharan dust measured by the C-130 aircraft during SHADE: 1. Solar spectrum, J. Geophys. Res., 108(D18), 8577, doi:10.1029/2002JD002687, 2003.

Houweling, S. , Hartmann, W., Aben, I., Schrijver, H., Skidmore, J., et al.: Evidence of systematic errors in SCIAMACHY-observed CO_2 due to aerosols, Atmos. Chem. Phys., 5, 3003–3013, 2005, http://www.atmos-chem-phys.net/5/3003/2005/.

Jongma, R. T., Gloudemans, A. M. S., Hoogeveen, R. W. M., Aben, I., de Vries, J., Escudero-Sanz, I., van den Oord, G. H. J., and Levelt, P. F.: Sensitivity analysis of a new SWIR-channel measuring tropospheric CH_4 and CO from space, in: Imaging Spectrometry XI, edited by: Shen, S. S. and Lewis, P. E., Proceedings of SPIE, 6302, 630214, 2006.

Kahn, R. A., Gaitley, B. J., Martonchik, J. V., Diner, D. J., Crean, K. A., and Holben, B.: Multiangle Imaging Spectroradiometer (MISR) global aerosol optical depth validation based on 2 years of coincident Aerosol Robotic Network (AERONET) observations, J. Geophys. Res., 110, D10S04, doi:10.1029/2004JD004706, 2005.

Karyampudi, V. M., Palm, S. P., Reagan, J. A., Fang, H., Grant, W. B., Hoff, R. M., Moulin, C., Pierce, H. F., Torres, O., Browell, E. V., and Harvey Melfi, S.: Validation of the Saharan dust plume conceptual model using lidar, Meteosat, and ECMWF data, B. Am. Meteorol. Soc., 80, 1045–1075, 1999.

Kelder, H., van Weele, M., Goede, A., et al.: CAPACITY: composition of the atmosphere: progress to applications in the user community, Final report, ESA reference 17237/03/NL/GS, October 2005.

Kleipool, Q.: SCIAMACHY SODAP: Algorithm specification for dark signal determination, Tech. Report SRON-SCIA-PhE-RP-009, SRON, 2003a.

Kleipool, Q.: SCIAMACHY: Recalculation of OPTEC5 nonlinearity, Tech. Report SRON-SCIA-PhE-RP-013, SRON, 2003b.

Kleipool, Q.: SCIAMACHY: Orbital variation of dark signal, Tech. Report SRON-SCIA-PhE-RP-18, SRON, 2004a.

Kleipool, Q.: SCIAMACHY: Evolution of dead and bad pixel mask, Tech. Report SRON-SCIA-PhE-RP-21, SRON, 2004b.

Kleipool, Q. L., Jongma, R., Gloudemans, A. M. S., et al.: In-flight proton-induced radiation damage to SCIAMACHY's extended-wavelength InGaAs near-infrared detectors, Infrared Phys. Technol., 50, 30–37, 2007.

Krijger, J. M., Aben, I., and Schrijver, H.: Distinction between clouds and ice/snow covered surfaces in the identification of cloud-free observations using SCIAMACHY PMDs, Atmos. Chem. Phys., 5, 2729–2738, 2005, http://www.atmos-chem-phys.net/5/2729/2005/.

Lichtenberg, G., Kleipool, Q., Krijger, J. M., van Soest, G., van Hees, R., Tilstra, L. G., Acarreta, J. R., Aben, I., Ahlers, B., Bovensmann, H., Chance, K., Gloudemans, A. M. S., Hoogeveen, R. W. M., Jongma, R. T. N., Noël, S., Piters, A., Schrijver, H., Schrijvers, C., Sioris, C. E., Skupin, J., Slijkhuis, S., Stammes, P., and Wuttke, M.: SCIAMACHY Level 1 data: calibration concept and in-flight calibration, Atmos. Chem. Phys., 6, 5347–5367, 2006, http://www.atmos-chem-phys.net/6/5347/2006/.

Rondeaux, G. and Herman, M.: Polarization of light reflected by crop canopies, Remote Sens. Environ., 38, 63–75, 1991.

Rothman, L. S., Jacquemart, D., Barbe, A., et al.: The HITRAN 2004 molecular spectroscopic database, J. Quant. Spectr. Radiat. Trans,, 96, 139–204, 2005.

Schrijver, H.: Retrieval of carbon monoxide, methane and nitrous oxide from SCIAMACHY measurements, in Proc. ESAMS, European Symposium on Atmospheric Measurements from Space, ESA WPP-161 1, ESTEC, Noordwijk, The Netherlands, 285–294, 1999.

Schrijver, H., Gloudemans, A. M. S., Houweling, S., and Aben, I.: Comparison of two years of methane column retrievals from SCIAMACHY observations in the 1.65 and 2.33 micrometer windows, in: Proc. Atmospheric Science Conference, ESA-SP 628, 8–12 May 2006, Frascati, Italy, p.23.1, 2006.

Schrijver, H.: Validation of SCIAMACHY channel 8 calibrations in the level 1B validation data set, in: Proc. of the Third Workshop on the Atmospheric Chemistry Validation of Envisat (ACVE-3), ESA-SP 642, 4–7 December 2006, Frascati, Italy, p., 2007.

Tie, X., Madronich, S., Walters, S., Edwards, D. P., Ginoux, P., Mahowald, N., Zhang, R., Lou, C., and Brasseur, G.: Assessment of the global impact of aerosols on tropospheric oxidants, J. Geophys. Res., 110, D03204, doi:10.1029/2004JD005359, 2005.

Torres, O., Decae, R., Veefkind, P., and de Leeuw, G.: OMI aerosol retrieval algorithm, ATBD-OMI-03, 47–69, 2001.